TÜBİTAK

Turkish Journal of Chemistry

http://journals.tubitak.gov.tr/chem/

Research Article

Turk J Chem
(2015) 39: 970 – 983

doi:10.3906/kim-1501-71

# Influence of acid and heavy metal cation exchange treatments on methane adsorption properties of mordenite

**Meryem SAKIZCI**[1,*], **Leyla ÖZGÜL TANRIVERDİ**[2]
[1]Department of Physics, Faculty of Science, Anadolu University, Eskişehir, Turkey
[2]Graduate School of Science, Anadolu University, Eskişehir, Turkey

**Received:** 21.01.2015 • **Accepted/Published Online:** 02.06.2015 • **Printed:** 30.10.2015

**Abstract:** In this study, the adsorption of methane ($CH_4$) capacities onto natural mordenite obtained from İzmir, Turkey, and its cationic forms (CuM, AgM, FeM, and HM samples) were investigated at the temperatures of 0 and 25 °C up to 100 kPa. Natural and modified samples were characterized by X-ray diffraction (XRD), X-ray fluorescence (XRF), Fourier transform infrared (FT-IR), thermogravimetry (TG-DTG), differential thermal analysis (DTA), scanning electron microscopy (SEM) coupled with energy dispersion spectroscopy (EDS), and $N_2$ adsorption methods. Quantitative XRD analysis showed that the major component of the natural zeolite was mordenite, together with minor amounts of quartz, feldspar, and clay mineral. The specific surface area and microporosity of the mordenite sample decreased notably after Ag cation exchange treatment. It was found that the adsorption capacity and the affinity of $CH_4$ with mordenite samples depended mainly on the type of exchanged cations and increased as HM < FeM < CuM < M < AgM for 25 °C. The uptake of methane increased as HM < FeM < CuM < AgM < M for 0 °C. Capacity of mordenites for $CH_4$ ranged from 0.237 mmol $g^{-1}$ to 0.528 mmol $g^{-1}$.

**Key words:** Adsorption, methane, mordenite, XRD, FT-IR, SEM-EDS, TG-DTG-DTA

## 1. Introduction

Mordenite is a kind of naturally occurring high-silica zeolite. It has an orthorhombic unit cell with idealized chemical formula $Na_8(AlO_2)_8(SiO_2)_{40}.24H_2O$. Mordenite has two different types of pore channels. One is composed of a 12-membered channel (6.5 Å × 7.0 Å) running along the c-axis, and the other is an 8-membered channel (2.6 Å × 5.7 Å) running along the b-axis in the form of small side pockets. Eight-ring side pockets of 3.4 Å × 4.8 Å have obstructions that essentially prohibit mobility of molecules from one main channel to the other.[1] Thus, the channel system is mainly 2-dimensional pores with 12-membered elliptical channels and a limiting diffusion in the [010] or b-axis.[2,3] The physical and chemical properties of natural zeolites can be improved by several methods such as acid treatment, ion exchange, and surfactant functionalization.[4–7] In general, acid treatment of natural zeolite may remove impurities that block the pores, progressively eliminate cations to change into H-form, and finally delaminate the structure. The removal of alumina in the mordenite zeolite causes enlargement of pore sizes in both the main channels and side pockets, and these effects are more detectable in the side pockets than in the main channels.[8–13]

Methane is the primary component of natural gas that occurs as a result of the decomposition of plant or

*Correspondence: msakizci@anadolu.edu.tr

organic matter in the absence of oxygen. It is present in the atmosphere at low concentrations and is the second most important greenhouse gas that contributes to global climate change.[14] Methane emissions are emitted from industrial processes, fossil fuel extraction, coal mines, incomplete fossil combustion, and garbage decomposition in landfills.[15,16] $CH_4$ has no dipole or quadrupole moment and it has a high polarizability constant (2.60 $Å^3$).[17] The electron cloud of the $CH_4$ molecule has apparent ability to be polarized by a positive charge center. The adsorption of methane molecules on solid surfaces is primarily due to nonspecific interaction (i.e. dispersion plus polarization). The dispersion interaction increases with the polarizabilities of the adsorbate and the solid surface. The polarization interaction increases with the polarizability of the adsorbate and the electric field on the solid surface.[18,19] Clays, bentonites, zeolites, carbons, polymeric resins, and silicas and their modified materials have been used for $CH_4$ adsorption.[10,19,20–35] Some of the most effective materials for adsorption of $CH_4$ are carbons. The packing density is a very significant factor to obtain a high volumetric storage capacity of methane. Zeolites have higher packing densities than carbons. Therefore, the search for other materials with methane adsorption capability has focused considerable attention on zeolites. However, studies on adsorption of $CH_4$ based on natural and modified zeolites from Turkey are very limited in the literature. Ackley and Yang[22,23] carried out a study on natural and modified forms of clinoptilolite and proposed that the adsorption capacities of $CH_4$ and $N_2$ depended on the type, size, number, and location of the cation, giving the following order of $CH_4$ adsorption on natural and modified clinoptilolites: $Ca^{2+} < Na^+ < Mg^{2+} <$ Nat. $< H^+ < K^+$. $CH_4$ adsorption capacities of Na- and H-forms of mordenite samples at –22.5 and 23 °C were measured using a volumetric apparatus.[10] Aguilar-Armenta et al.[30] investigated the adsorption kinetics of pure $CO_2$, $O_2$, $N_2$, and $CH_4$ on natural and cation-exchanged clinoptilolites at 20 °C. They found that the uptake of $CH_4$ decreased as Ca $\approx$ K $>$ Nat. $>$ Na for clinoptilolite samples. Jayaraman et al.[31] measured the high-pressure adsorption isotherms and diffusion rates for nitrogen and methane on cation-exchanged clinoptilolites at 22 °C. They showed that $CH_4$ adsorption of clinoptilolite samples decreased in the order of $Na^+ > H^+ = K^+ > Mg^{2+} >$ Nat. $> Li^+ > Ca^{2+}$. Delgado et al.[19] obtained the adsorption equilibrium isotherms of $CO_2$, $CH_4$, and $N_2$ on Na- and H-mordenite at pressures of up to 2 MPa at three temperatures (6, 20, and 35 °C). They found that the adsorption of methane by Na-mordenite was higher than that exhibited by H-mordenite, resulting from the smaller electric field in H-mordenite. Kouvelos et al.[32] measured the high-pressure nitrogen and methane adsorption isotherms of natural and monovalent ($Li^+$ and $Na^+$) cation-exchanged clinoptilolite at 0 and 25 °C and reported that the adsorption and kinetics characteristic of the clinoptilolite samples were affected significantly by the type and distribution of the charge-balancing cations. Faghihian et al.[33] studied the adsorption of $N_2$, $CH_4$, and $C_2H_6$ on natural clinoptilolite and on its cation-exchanged forms (Na, K, and H) at 25 °C and reported that the H-form could be effective as an adsorbent for $CH_4$ adsorption. Sun et al.[34] investigated the adsorption amount of methane on 16 different kinds of materials at 3.5 MPa and 298 K and reported that the adsorption capacity of these samples increased linearly with the specific surface area. Shang et al.[35] carried out a study on the behavior of potassium chabazite as a nanocontainer to $N_2$ and $CH_4$ and reported that the adsorption of $CH_4$ on potassium chabazite (KCHA1) at 6 °C and 1 M Pa amounted to 1.97 mmol $g^{-1}$.

The aim of the present study is to investigate the effect of the acid and heavy metal cation-exchange treatments on structural, thermal, and methane adsorption properties of the mordenite samples.

## 2. Results and discussion

### 2.1. Materials and chemicals

The mordenite sample was obtained from İzmir, Turkey. The zeolite samples were air-dried at room temperature and ground to pass through a sieve of $\leq 45$ $\mu$m. Cationic forms of mordenite (AgYZ, CuYZ, FeYZ, and HYZ) were prepared by using 1 M solutions of $Fe(NO_3)_3.9H_2O$, $AgNO_3$, $Cu(NO_3)_2.3H_2O$, and HCl at 80 °C for 6 h. After the modified processes, the treated samples were rinsed with deionized water and then dried at room temperature. Before the experimental procedure, all samples were dried in an oven at 110 °C for 16 h and stored in a desiccator.

Inorganic chemicals such as HCl, $Fe(NO_3)_3.9H_2O$, $AgNO_3$, and $Cu(NO_3)_2.3H_2O$ were supplied by Merck (Darmstadt, Germany) and all solutions were prepared by using deionized water.

### 2.2. Instrumentation

Chemical compositions were determined on powdered samples fused with lithium tetraborate using X-ray fluorescence analysis (XRF; Rigaku ZSX Primus instrument). The X-ray diffraction (XRD) diffractograms were obtained with a D8 Advance Bruker AXS instrument, using $CuK_\alpha$ radiation ($\lambda = 1.54$ Å) at 40 kV and 20 mA in the range of 3–50° $2\theta$. The samples were scanned with a $2\theta$ step of 0.02°. Thermal analysis was carried out using a Setsys Evolution Setaram TG/DTA apparatus (range: 30–1000 °C) under flowing nitrogen (20 mL $min^{-1}$) at a heating rate of 10 °C $min^{-1}$ using ~30 mg of samples in alumina crucibles. An empty alumina crucible (100 $\mu$L) was used as a reference and heat flow between the sample and the reference was recorded. Infrared spectra of the mordenite samples were recorded in the region of 4000–400 $cm^{-1}$ via a Bruker-Vertex 80v FT-IR spectrometer at a resolution of 4 $cm^{-1}$ using the KBr pellet technique. The morphological forms and elemental compositions were determined by means of a scanning electron microscopy (SEM) with a JEOL JSM-6510LV equipped with a system for elemental composition analysis based on energy dispersive spectroscopy (INCA EDS; Oxford Instruments). Images of the sample surfaces were recorded at different magnifications. Elemental analysis was performed at different points randomly selected on the sample surface and the average of the results was reported.

The textural characteristics of the samples were measured with automated Autosorb 1-C volumetric equipment (Quantachrome Instruments, Boynton Beach, FL, USA) using nitrogen gas adsorption at –196 °C. Before each measurement the samples were degassed at 300 °C for 7 h. The specific surface areas were calculated according to the standard Brunauer–Emmett–Teller (BET) method. The BET gas adsorption method is the most widely used standard procedure for the calculation of the specific surface of solids and involves the use of the BET equation[36] (Eq. (1)):

$$\frac{1}{V\left[(P_0/P)-1\right]} = \frac{1}{V_m C} + \frac{C-1}{V_m C}\left(\frac{P}{P_0}\right) \tag{1}$$

where $P_o$ is the saturated vapor pressure of the gas over the solid, $P/P_o$ is the relative pressure of the adsorbate, and C is the so-called BET C-constant. $V_m$ is the amount adsorbed at the relative pressure $P/P_o$ and is the monolayer capacity. The BET surface areas of the natural zeolite and modified natural zeolites were calculated using the adsorption isotherm in the range of relative pressure from 0.03 to 0.2. The micropore area and volume were calculated by the $t-$plot method.[37] The De Boer model was applied for micropore size calculations. The cumulative pore volume and average pore diameter were calculated using the adsorption data by the density functional theory model. High-purity (99.99%) nitrogen was used as the adsorbate. Retention

values of methane by zeolite samples were determined using automated Autosorb 1-C volumetric equipment (Quantachrome Instruments) at 0 and 25 °C up to 100 kPa. About 0.1 g of the sample was outgassed in a vacuum at 300 °C for 7 h before methane adsorption.

## 3. Experimental

### 3.1. Chemical analysis

The chemical compositions of the natural and modified mordenite samples are listed in Table 1. The XRF analysis results showed a high composition of silicon (Si) in all natural zeolites (Table 1). Mordenite is defined as a K-rich mineral due to its highest $K^+$ content.[38] Upon ion exchange with heavy metal cations, $K^+$ can only be partially removed since the removal of $K^+$ depends on its source. The most noticeable property of the heavy metal cation-exchange process was the high selectivity of mordenite for $Ag^+$ cations.

**Table 1.** Chemical analyses of oxides (%) for natural and modified mordenite samples.

| Chemical analysis (%) | M | CuM | FeM | AgM | HM |
|---|---|---|---|---|---|
| $SiO_2$ | 71.518 | 70.131 | 73.319 | 69.102 | 74.299 |
| $Al_2O_3$ | 12.866 | 13.325 | 12.336 | 12.696 | 12.065 |
| $Fe_2O_3$ | 1.121 | 1.098 | 1.461 | 1.021 | 0.799 |
| MgO | 0.190 | 0.113 | 0.145 | 0.138 | 0.107 |
| CaO | 1.267 | 0.607 | 0.784 | 0.129 | 0.706 |
| $K_2O$ | 5.366 | 5.096 | 5.104 | 4.601 | 5.273 |
| $Na_2O$ | 1.045 | 0.766 | 0.663 | 0.298 | 0.527 |
| $TiO_2$ | 0.094 | 0.112 | 0.120 | 0.084 | 0.097 |
| CuO | - | 1.472 | - | - | - |
| $Ag_2O$ | - | - | - | 5.635 | - |
| Others | 0.004 | 0.005 | 0.005 | 0.005 | 0.003 |
| LOI | 6.529 | 7.275 | 6.063 | 6.291 | 6.124 |
| $SiO_2/Al_2O_3$ | 5.55 | 5.26 | 5.94 | 5.44 | 6.15 |

At acid treatment by 1 M HCl solution, the mordenite zeolite sample is subject to dealumination and removal of cations without significant destruction of the crystal lattice in comparison with the natural zeolite. This is consistent with a number of studies where mordenite-type zeolites have been shown to be insignificantly dealuminated by HCl.[39–41] Acid treatment increases the $SiO_2/Al_2O_3$ molar ratio from 5.55 to 6.15 by removing aluminum from the zeolite structure.[11,42] Moreover, a decrease in the compensating cation content (Ca, Na, and Mg) is observed. On the other hand, the removal of potassium with HCl solution is at a low rate due to the significant amount of potassium originating from K-feldspar, which is insoluble in HCl solution.[13]

### 3.2. X-ray analysis

The XRD patterns of all mordenite samples are shown in Figure 1. The characterization results indicated that the Turkish natural mordenite consisted mainly of mordenite. The characteristic peaks of mordenite were observed at $2\theta = 9.73°$, $15.23°$, $19.57°$, $22.26°$, $25.67°$, and $27.66°$, respectively.[3,11,43] In addition to the mordenite phase, minor amounts of feldspar, quartz, and clay mineral were also present in the zeolite sample.

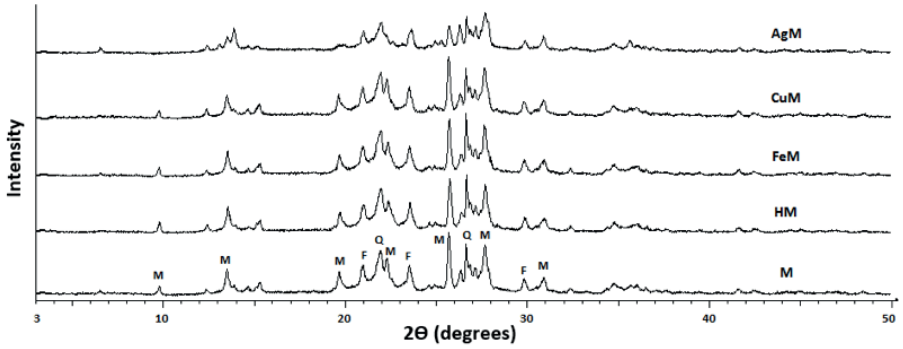


**Figure 1.** XRD patterns of natural and modified mordenite samples (M, mordenite; F, feldspar; Q, quartz).

In general, the overall x-ray investigation of modified mordenite samples showed that it did not lead to significant structural changes. Nevertheless, the XRD pattern of the AgM sample was affected to some extent and showed significant changes in characteristic peak intensities of mordenite. The peaks $2\theta = 9.73°$ and $22.26°$ corresponding to mordenite disappeared in the AgM sample. After the treatment of the mordenite sample with silver nitrate solution, the mordenite reflection at $19.57°$ was still present but its intensity decreased considerably. The decrease in the peak intensities at $15.23°$, $19.57°$, and $25.67°$ $2\theta$ attributed to framework cations was probably caused by the compositional change within the mineral after the exchange. Natural zeolites have good selectivity for silver ions.[44,45]

The comparative analysis of the powder patterns of both the natural form and the H-form of mordenite showed that there are no visible changes in the peak intensities after modification (Figure 1). These results confirm the XRF data. Minor Al leaching is observed after acid treatment of natural mordenite (Table 1). The presence of mordenite and quartz in the natural zeolites increases their stability towards ion exchange and acid leaching. These results are in line with results obtained by other authors.[12,13]

### 3.3. Thermal properties

The thermogravimetric (TG-DTG) and differential thermal analysis (DTA) curves of all forms of mordenite samples are presented in Figure 2. In addition, the percentage of water molecules removed in the samples is summarized in the temperature intervals of 30–200 °C, 200–400 °C, 400–700 °C, and 700–1000 °C, as seen in Table 2. As seen in Figure 2, the curves of natural and modified samples are similar. The DTA curves of natural and modified mordenite samples exhibited only two endothermic peaks (Figure 2). The most remarkable maximum occurs at 109–139 °C, while the other at 500–513 °C is weaker. These peaks indicate gradual dehydration involving the water molecules present in different structural positions.[46]

**Table 2.** Mass loss (%) of the mordenite samples used at different temperature ranges.

| Sample | 30–200 °C | 200–400 °C | 400–700 °C | 700–1000 °C | Tot. (%) |
|---|---|---|---|---|---|
| M | 3.10 | 1.38 | 1.48 | 0.10 | 6.06 |
| AgM | 2.93 | 1.35 | 1.37 | 0.12 | 5.77 |
| CuM | 3.20 | 1.64 | 1.73 | 0.16 | 6.73 |
| FeM | 3.81 | 1.27 | 1.55 | 0.27 | 6.90 |
| HM | 3.01 | 1.17 | 1.47 | 0.35 | 6.00 |

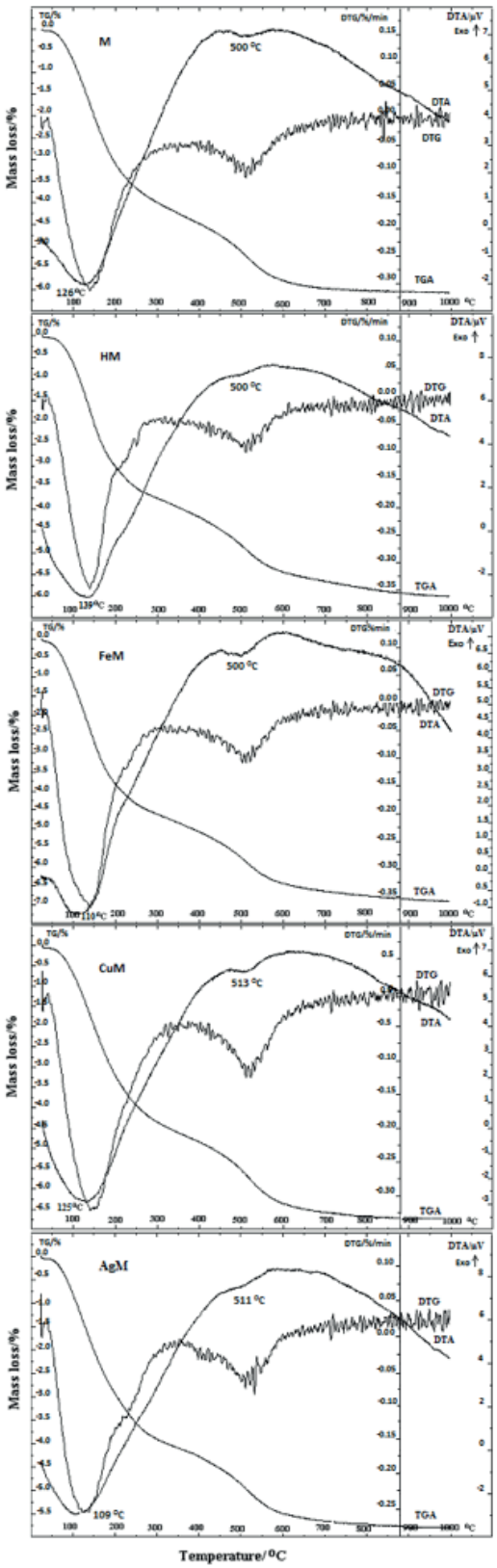


**Figure 2.** TG-DTG and DTA curves natural and modified mordenite samples.

Mordenite zeolite is stable at temperatures of up to 800 °C, while further increases in temperature lead to structural changes due to conversion of its structure to another crystal or amorphous phase.[47] High Si/Al ratio and the presence of $K^+$ ions favored an increase in the stability of the crystal structure upon heating. The TG curves of zeolite samples (Figure 2) showed two stages of dehydration of natural mordenite. Zeolitic water can be removed by heating to approximately 400 °C. The mass loss at this temperature reaches 4.18%–5.08%. The total mass loss while heating zeolite up to 700 °C is 5.65%–6.63%. Water release in zeolite proceeds continuously and smoothly, as evidenced by the mass loss (TG) curve. The iron-modified mordenite gave the highest rate of weight loss. The total mass losses of AgM, HM, M, CuM, and FeM were determined as 5.77%, 6.00%, 6.06%, 6.73%, and 6.90%, respectively.

### 3.4. FT-IR analysis

There are two categories of frequencies of vibration in the FT-IR spectrum of the zeolites. The first category of vibrations arises due to internal vibrations of the $TO_4$ tetrahedron, which is the primary unit of the structure and is not sensitive to other structural units. The second category of vibrations is associated with the external linkage between tetrahedrals.[47] The FT-IR spectra of natural and exchanged forms of mordenite samples were investigated in the region of 4000–400 $cm^{-1}$ (Table 3; Figure 3).

**Table 3.** The exact position (peak wavenumber) of bands observed in FT-IR for natural and modified zeolites.

| Sample | Ti-O stretching vibration | | T-O bending mode (-$SiO_4$-) | OH-stretching mode | OH-bending mode | Other |
|---|---|---|---|---|---|---|
| | Zeolite | ($SiO_2$) | | | | |
| M | 1045 | 793 | 470 | 3695, 3620 | 1633 | 703, 580, 536 |
| AgM | 1062 | 794 | 468 | 3697, 3620 | 1633, 1423 | 705, 582, 538 |
| CuM | 1051 | 794 | 468 | 3695, 3620 | 1637 | 702, 582, 538 |
| FeM | 1066 | 793 | 466 | 3695, 3620 | 1637, 1506, 1440 | 705, 582, 534 |
| HM | 1066 | 794 | 468 | 3695, 3620 | 1633 | 705, 582, 538 |

As shown in Figure 3, cation exchange of zeolites did not lead to distinct shifts in the positions of the bands in the FT-IR spectra. Mordenite zeolite gives a strong T-O stretching vibration band in the range of 1045–1070 $cm^{-1}$ (Table 3).[48–50] Other bands appear near 794 and 470 $cm^{-1}$. The band at ∼794 $cm^{-1}$ appears in all spectra and can be attributed to quartz or amorphous $SiO_2$, which is consistent with the XRD patterns of mordenite samples (Figure 1). A weak band at 466–470 $cm^{-1}$ can be assigned to a clay sample or other Si-O-Si bending vibration.[48,49] The band at ∼538 $cm^{-1}$ can be attributed to feldspar.[51]

The bands in the region of 1600–3700 $cm^{-1}$ can be attributed to the presence of zeolitic water (Table 3; Figure 3). There are several types of zeolitic water as seen as in TG (Figure 2). Isolated $OH^-$ stretching at 3620 $cm^{-1}$ for all zeolite samples was observed. This band is assigned to the interaction between the water hydroxyl and cations. After Ag-exchange treatment of zeolite with nitrate solution, the intensities of the bands at 3695 and 3620 $cm^{-1}$ decreased because of decationization and dealumination from the structure of zeolite as shown from XRF and XRD (Table 1; Figure 1). The H-O-H bending frequency of the water molecules occurs at 1633–1637 $cm^{-1}$ with a medium intensity in the infrared spectra.[43,48–50] In the region of 600–800 $cm^{-1}$, the bands are attributed to exchangeable cations and are due to pseudolattice vibrations of structural units.[52,53]

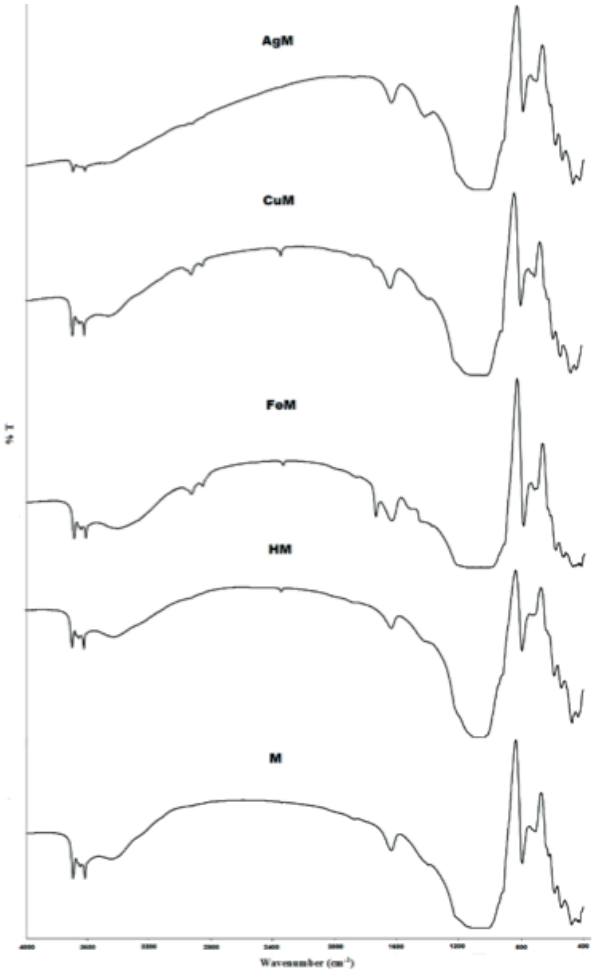


**Figure 3.** FT-IR spectra of natural and modified mordenite samples.

### 3.5. SEM/EDS analysis

SEM analysis was used to reveal the morphology of mordenite samples. SEM microimages indicated that mordenite has a needle-like crystal structure (Figures 4–6). Characteristic observations from SEM analysis included crystalline mordenite, feldspar, quartz, and clay mineral. The SEM results are consistent with the XRD results. It was noted that the cation-exchanged forms of zeolites did not show any surface or morphological differences with respect to the natural mordenite sample.

The elemental compositions of the mordenite sample and its cationic forms were determined using EDS performed with 2 different random points. As Table 4 shows, the major elements of the natural mordenite sample were O, Si, Al, and K in addition to small amounts of Na and Ca. Mordenite is poor in Na and Ca and rich in K. It can be seen from Table 4 that the amount of Ca and Na was reduced after surface modifications. Besides the presence of major elements such as Si, Al, O, and K, copper is also identified in the CuM sample. EDS analysis showed the presence of Si, Al, O, K, and Ag in the AgM sample. In the EDS analysis of the FeM sample a significant atomic quantity of iron appears (Table 4).

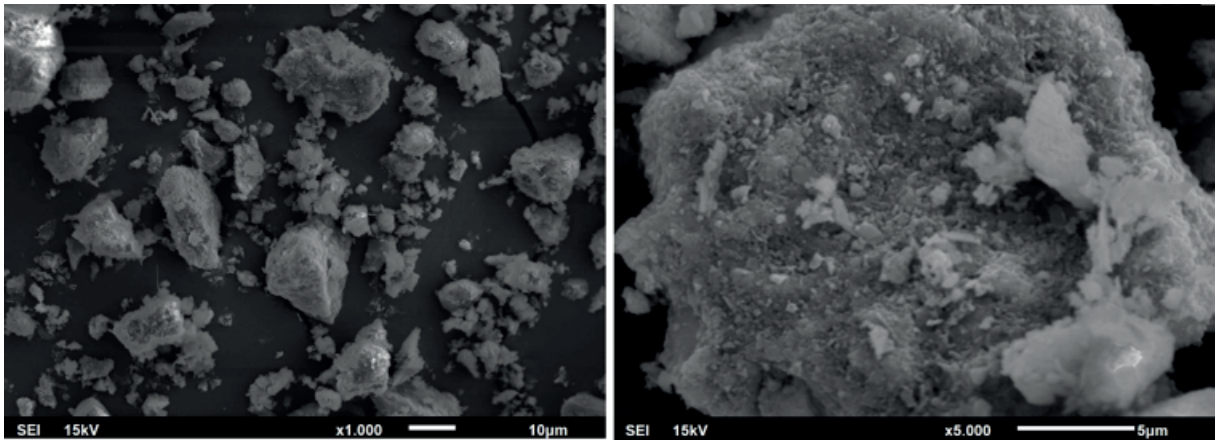


**Figure 4.** SEM images of natural mordenite sample.

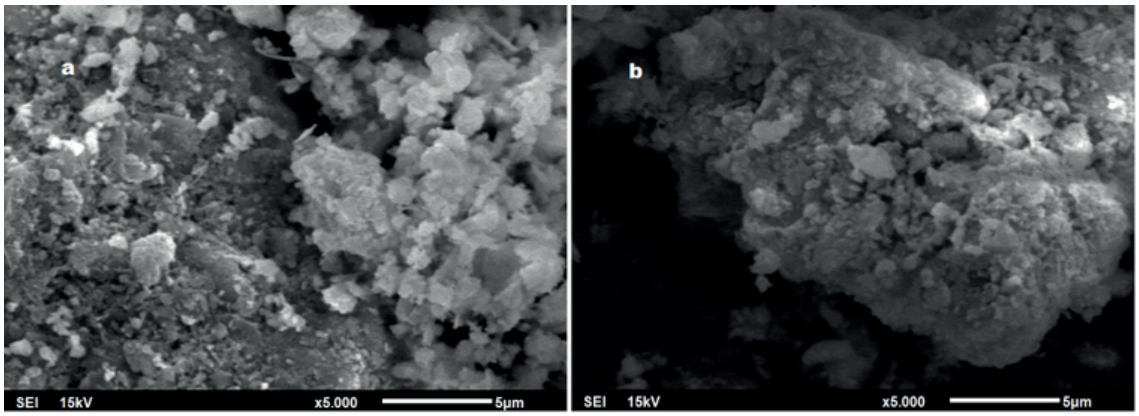


**Figure 5.** SEM images of (a) Ag- and (b) Fe-modified mordenite samples.

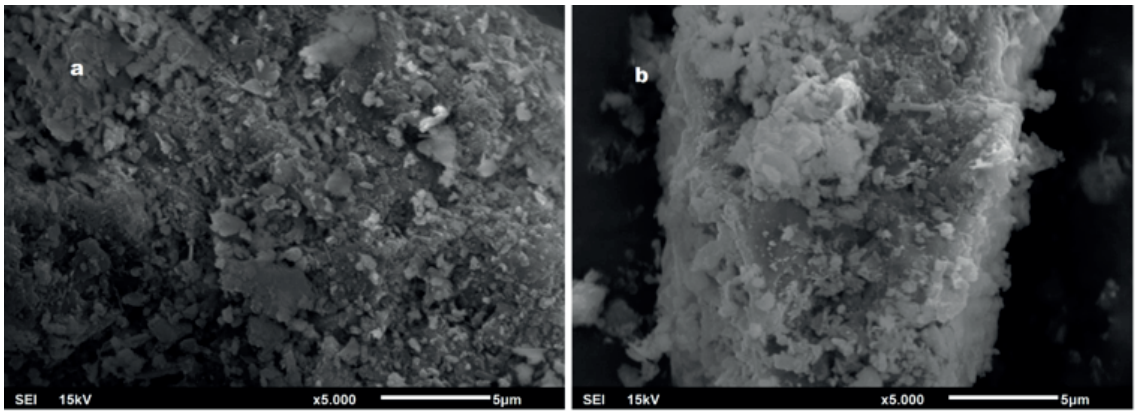


**Figure 6.** SEM images of (a) Cu- and (b) H-modified mordenite samples.

### 3.6. Specific surface area

The nitrogen adsorption isotherms of the natural zeolite and modified natural zeolites are shown in Figure 7. The adsorption isotherms of samples are of type II according to the IUPAC classification.[54] $N_2$ adsorption data of natural and modified mordenite samples are given in Table 5. Sample modifications by cation exchange are

modified micropore volume, micropore area, average pore diameter, and surface area results. It is evident that the silver and copper in the mordenite channels caused a decrease of specific surface area, micropore volume, micropore area, and increase of average pore diameter as compared with the natural mordenite. In the case of 1 M silver nitrate treatment, the specific surface area of the natural sample (M) decreased from 93 $m^2\ g^{-1}$ to 73 $m^2\ g^{-1}$ and the average pore diameter of the natural sample (M) increased from 46.08 Å to 80.19 Å (Table 5). The decrease in specific surface areas of AgM can be attributed to partial blocking of the channels in the presence of $Ag^+$ cations. Munakata[55] showed that ionic exchange with silver nitrate of mordenite decreased the specific surface area from 217 to 109 $m^2\ g^{-1}$.

**Table 4.** Average elemental composition of mordenite and modified zeolites.

| Element, at. % | M | CuM | FeM | AgM | HM |
|---|---|---|---|---|---|
| O | 60.47 | 58.38 | 58.37 | 61.45 | 48.88 |
| Al | 5.00 | 6.27 | 5.63 | 5.85 | 5.72 |
| Si | 30.36 | 31.39 | 27.88 | 29.13 | 42.28 |
| Fe | - | 0.18 | 5.07 | - | - |
| Ca | 0.50 | 0.10 | 0.26 | - | 0.34 |
| K | 3.15 | 2.45 | 2.40 | 1.83 | 2.48 |
| Na | 0.52 | 0.20 | 0.39 | - | 0.30 |
| Cu | - | 1.03 | - | - | - |
| Ag | - | - | - | 1.74 | - |

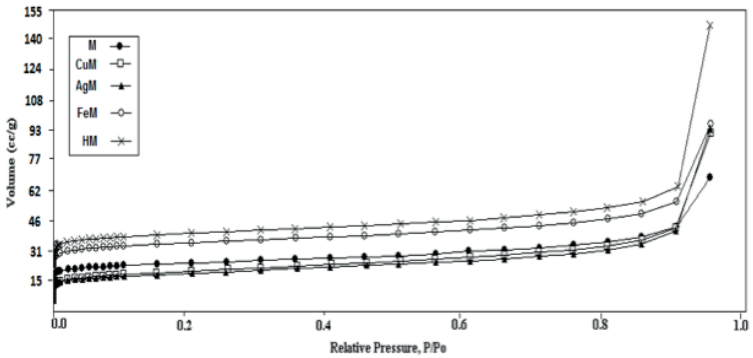


**Figure 7.** $N_2$ adsorption isotherms of natural and modified mordenite samples.

**Table 5.** $N_2$ and $CH_4$ adsorption data of natural and modified mordenite samples.

| Sample | Amount adsorbed (mmol $g^{-1}$) | | BET surface area ($m^2\ g^{-1}$) | Micropore volume ($cm^3\ g^{-1}$) | Micropore area ($m^2\ g^{-1}$) | Cumulative pore volume ($cm^3\ g^{-1}$) | Average pore diameter (Å) |
|---|---|---|---|---|---|---|---|
| | 0° C | 25° C | | | | | |
| M | 0.528 | 0.339 | 93 | 0.027 | 67.09 | 0.098 | 46.08 |
| AgM | 0.498 | 0.372 | 73 | 0.015 | 37.91 | 0.133 | 80.19 |
| CuM | 0.449 | 0.295 | 77 | 0.016 | 38.39 | 0.129 | 73.58 |
| FeM | 0.398 | 0.269 | 132 | 0.041 | 103.39 | 0.136 | 45.56 |
| HM | 0.384 | 0.237 | 149 | 0.047 | 120.58 | 0.205 | 61.28 |

On the other hand, the acid treatment of natural mordenite increased the specific surface area, micropore volume, micropore area, and Si/Al ratio as shown as Tables 1 and 5. The highest value of HM surface area

could be related to the amorphous material dissolution that could block zeolite structure channels, generating new ones.[11,41,42] In addition, replacement of exchangeable cations with the much smaller $H^+$ caused an increase of the specific surface area as compared with the natural sample. The $N_2$ volume adsorbed at the highest $P/P_o$ for HM is found as 18.26 $cm^3\ g^{-1}$. Surface area was found as 149 $m^2\ g^{-1}$ from BET. Similarly, Fe modification of the mordenite sample resulted in increased specific surface area. The specific surface area of the mordenite sample increased from 93 $m^2\ g^{-1}$ to 132 $m^2\ g^{-1}$ after cation exchange with the iron nitrate solution of the zeolite sample. As the micropore volume increased from 0.027 $cm^3\ g^{-1}$ to 0.047 $cm^3\ g^{-1}$ the average pore diameter decreased from 46.08 Å to 45.50 Å (Table 5).[12,56]

### 3.7. Adsorption of $CH_4$

The adsorption isotherms for methane on natural and modified mordenite samples at 0 °C and 25 °C were obtained at pressures up to 100 kPa. The adsorption temperatures of $CH_4$ were above the critical temperature (Tc = –82.6 °C). The adsorption isotherms (absolute amount adsorbed per gram of adsorbent) of $CH_4$ on all the samples are shown in Figures 8 and 9. As shown in Figures 8 and 9 and listed in Table 5, the adsorption capacity and the affinity of $CH_4$ with the zeolite samples differed depending on the cations exchanged. In addition, the amount of adsorbed $CH_4$ increased with decreasing temperature, as expected. Capacity of mordenites for $CH_4$ ranged from 0.237 mmol $g^{-1}$ to 0.528 mmol $g^{-1}$ (Table 5).

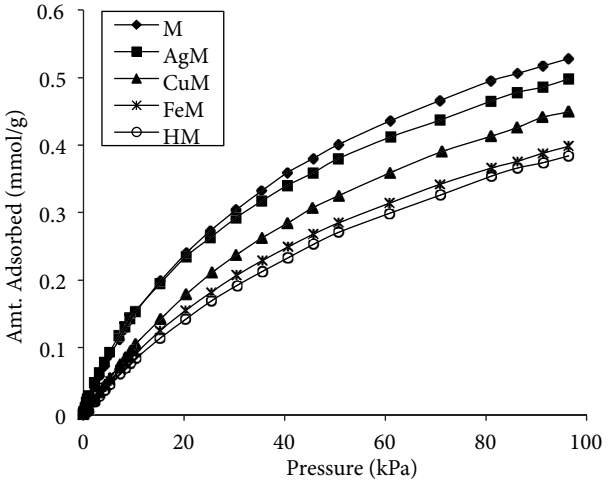


**Figure 8.** Adsorption of methane on mordenite zeolites at 0 °C.

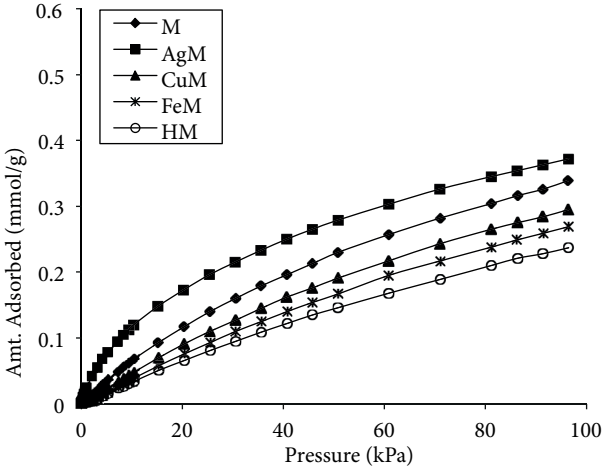


**Figure 9.** Adsorption of methane on mordenite zeolites at 25 °C.

It can be noted that natural mordenite zeolite showed much higher methane adsorption compared to the modified forms at 0 °C and 100 kPa. The kinetic diameter of methane (3.8 Å) is small enough for diffusion of this molecule inside mordenite zeolite pore openings. It was observed that uptake of methane on mordenite zeolite at 0 °C increased in the following sequence (Figures 8 and 9): HM < FeM < CuM < AgM < M.

The amount of adsorbed $CH_4$ was influenced by the exchangeable cation at 25 °C and increased in the order of HM < FeM < CuM < M < AgM. The difference in adsorption capacities is likely due to the strength of adsorption sites. Among all the modified zeolites, the Ag-form exhibited the best properties in terms of adsorption capacity at both temperatures. As seen from Table 5, adsorption capacity of $CH_4$ on AgM increases considerably as the temperature is decreased. From 25 °C to 0 °C, $CH_4$ adsorption amount is increased from

0.372 mmol $g^{-1}$ to 0.498 mmol $g^{-1}$ for AgM. For AgM, the high $CH_4$ adsorption capacity can be attributed to both stronger electrostatic and polarization interactions. At 0 °C, the $CH_4$ adsorption capacity of the CuM sample is found to be 0.449 mmol $g^{-1}$. Among the heavy metal cation-exchanged zeolite samples, the Fe-form exhibited the lowest adsorption capacity for $CH_4$. This could be due to the clogging effect of impurities during heavy metal treatment or due to the formation of extra-framework aluminum upon calcination. At 0 °C, the amount of $CH_4$ retained by the FeM sample was 0.398 mmol $g^{-1}$, whereas the corresponding value was 0.269 mmol $g^{-1}$ at 25 °C. The electrostatic field is affected by the presence of the exchangeable cations.[57]

The H-form for both temperatures has been observed to have the lowest adsorption capacities for $CH_4$ gas. It has a value of 0.384 mmol $g^{-1}$ at 0 °C and 100 kPa (Table 5). The decrease of affinity to $CH_4$ of H-mordenite with respect to natural mordenite is remarkable. This decrease can be attributed to both weaker electrostatic and polarization interactions with the smaller electric field of the H-form.[19,57] The exchange of the metallic ions of zeolites with HCl results in the formation of silanol hydroxyl groups. These groups, though polar, lead to smaller field and field gradients than the cations, so that the intracrystalline environment is less polar in the H-form than in the Fe-, Cu-, and Ag-forms of mordenite.

## 4. Conclusion

In this study, characterization of mordenite samples (XRD, TG–DTA, FT-IR, SEM-EDS, and $N_2$ adsorption methods) and the efficiency of those of samples in the adsorption of methane have been investigated. XRD analysis demonstrated that appreciable change was observed in the crystallinity of natural zeolite after Ag-exchange treatment. Treatment of mordenite zeolite with 1 M silver and copper nitrate solutions led to decrease in the BET surface area, micropore volume, and micropore area. The Ag-exchanged zeolite exhibited the lowest surface area. The HCl treatment of the mordenite caused dealumination and dissolution of some amorphous materials increased its surface area. HM zeolite showed the biggest surface area among the zeolites. All modified mordenite samples exhibited a similar thermal behavior to natural mordenite.

In the case of $CH_4$ adsorption on modified zeolite samples at both temperatures, a better result is reached when AgM is used. The acid treatment of natural zeolite influenced the adsorption property of mordenite-rich tuff. The experimental data indicated that the HM adsorbent has the lowest adsorption capacity with respect to the adsorption of $CH_4$. The weaker interaction in HM is then attributed to both weaker electrostatic and polarization interactions. Ion-exchanged zeolites may cause considerable differences in the adsorption of methane due to both the location and size of the interchangeable cations, which affect the local electrostatic field, and the polarization of the adsorbates.

## Acknowledgments

This work was supported by an Anadolu University Commission of Scientific Research Project under grant no. 1306F165. Special thanks to Matthias Thommes for his helpful suggestions.

## References

1. Meier, W. M. *Z. Kristallogr.* **1961**, *115*, 439–450.
2. Hernandez, M. A. *Adsorption* **2000**, *6*, 33–45.
3. Baerlocher, C. H.; Meier, W. M; Olson, D. H. *Atlas of Zeolite Framework Types*, 5th ed.; Elsevier: Amsterdam, the Netherlands, 2001.

4. Rodríguez-Iznaga, I.; Petranovskii, V.; Rodríguez-Fuentes, G.; Bogdanchikova, N.; Avalos, M. *Stud. Surf. Sci. Catal.* **2001**, *135*, 212–212.
5. Inglezakis, V. J.; Loizidou, M. D.; Grigoropoulou, H. P. *Water Res.* **2002**, *36*, 2784–2792.
6. Orha, C.; Manea, F.; Ratiu, C.; Burtica, G.; Iovi, A. *Environm. Eng. Manag. J.* **2007**, *6*, 541–544.
7. Rodríguez-Iznaga, I.; Petranovskii, V.; Espinosa, M. A. H; Barraza, F. C.; Pestryakov, A. *Adv. Mat. Res.* **2014**, *880*, 48–52.
8. Meyers, B. L.; Fleisch, T. H.; Ray, G. J.; Miller, J. T.; Hall, J. B. *J. Catal.* **1988**, *110*, 82–95.
9. Sawa, M.; Niwa, M.; Murakami, Y. *Appl. Catal.* **1989**, *53*, 169–181.
10. Nagano, J.; Eguchi, T.; Asanuma, T.; Masui, H.; Nakayama, H.; Nakamura, N.; Derouane, E. G. *Micropor. Mesopor. Mater.* **1999**, *33*, 249–256.
11. Hernandez, M. A.; Petranovskii, V.; Avalos, M.; Portillo, R.; Rojas, F.; Lara, V. H. *Separation Sci. Technol.* **2006**, *41*, 1907–1925.
12. Viswanadham, N.; Kumar, M. *Micropor. Mesopor. Mater.* **2006**, *92*, 31–37.
13. Ates, A.; Hardacre, C. *J. Colloid Interf. Sci.* **2012**, *372*, 130–140.
14. Hengeveld, H.; Whitewood, B.; Fergusson, A. *Environment Canada*; Government of Canada: Downsview, Canada, 2005.
15. IPCC. In *Climate Change 2007: The Physical Basis. Contribution of Working Group I to the Fourth Assessment Report of the Intergovernmental Panel on Climate Change*; Solomon, S.; Qin, D.; Manning, M.; Chen, Z.; Marquis, M.; Averyt, K. B.; Tignor, M.; Miller, H. L., Eds. Cambridge University Press: Cambridge, UK, 2007, p. 996.
16. EPA. *Inventory of U.S. Greenhouse Gas, Emissions and Sinks*; Washington, DC, USA: EPA, 2013.
17. Yang, R. T. *Adsorbents: Fundamentals and Applications*; John Wiley & Sons Inc.: Hoboken, NJ, USA, 2003.
18. Barrer, R. M. *Zeolites and Clay Minerals as Sorbents and Molecular Sieves*; Academic Press: London, UK, 1978.
19. Delgado, J. A.; Uguina, M. A.; Gómez, J. M.; Ortega, L. *Sep. Purif. Technol.* **2006**, *48*, 223–228.
20. Munson, R. A.; Clifton, R. A. Jr. *Natural Gas Storage with Zeolites*; Washington, DC, USA: Bureau of Mines Nonmetallic Minerals Program, U.S. Department of the Interior, 1971.
21. Tan, Z.; Gubbins, K. E. *J. Phys. Chem.* **1990**, *94*, 6061–6069.
22. Ackley, M. W.; Yang, R. T. *Ind. Eng. Chem. Res.* **1991**, *30*, 2523–2530.
23. Ackley, M. W.; Yang, R. T. *AIChE J.* **1991**, *37*, 1645–1656.
24. Zhang, S. Y.; Talu, O.; Hayhurst, D. T. *J. Phys. Chem.* **1991**, *95*, 1722–1726.
25. Mullhaupt, J. T.; BeVier, W. E.; McMahon, K. C.; Van Slooten, R. A.; Lewis, I. C.; Grienke, R. A.; Strong, S. L.; Ball, D. R.; Steele, W. E. In *Carbon Adsorbents for Natural Gas Storage, Proceedings*; Essen, Germany, 1992.
26. Ioneva, M. A.; Newman, G. K.; Harwell, J. M. *AIChE Symp. Ser.* **1995**, *91*, 40–48.
27. Parkyns, N. D.; Quinn, D. F. In *Porosity in Carbons*; Patrick, J. W., Ed. Halsted Press: New York, NY, USA, 1995, pp. 291–325.
28. Menon, V. C.; Komarneni, S. *J. Porous Mat.* **1998**, *5*, 43–58.
29. Cook, T. L.; Komodromos, C.; Quinn, D. F.; Ragan, S. In *Carbon Materials for Advanced Technologies*; Burchell, T. D., Ed. Pergamon Press: New York, NY, 1999, pp. 269–302.
30. Aguilar-Armenta, G.; Hernandez-Ramirez, G.; Flores-Loyola, E.; Ugarte-Castaneda, A.; Silva-Gonzalez, R.; Tabares-Munoz, C.; Jimenez-Lopez, A.; Rodriguez-Castellon, E. *J. Phys. Chem. B* **2001**, *105*, 1313–1319.
31. Jayaraman, A.; Hernandez-Maldonado, A. J.; Yang, R. T.; Chinn, D.; Munson, C. L.; Mohr, D. H. *Chem. Eng. Sci.* **2004**, *59*, 2407–2417.
32. Kouvelos, E.; Kesore, K.; Steriotis, T.; Grigoropoulou, H.; Bouloubasi, D.; Theophilou, N.; Tzintzos, S.; Kanelopoulos, N. *Micropor. Mezopor. Mater.* **2007**, *99*, 106–111.

33. Faghihian, H.; Talebi, M.; Pirouzi, M. *J. Iran. Chem. Soc.* **2008**, *5*, 394–399.
34. Sun, Y.; Liu, C.; Su, W.; Zhou, Y.; Zhou, L. *Adsorption* **2009**, *15*, 133–137.
35. Shang, J.; Li, G.; Singh, R.; Xiao, P.; Liu, J. Z.; Webley, P. A. *J. Phys. Chem. C* **2010**, *114*, 22025–22031.
36. Brunauer, S.; Emmett, P. H.; Teller, E. *J. Amer. Chem. Soc.* **1938**, *60*, 309–319.
37. Lippens, B. C.; De Boer, J. H. *J. Catal.* **1965**, *4*, 319–323.
38. Pe-Piper, G.; Tsolis-Katagas, P. *Clays Clay Miner.* **1991**, *39*, 239–247.
39. Ghosh, A. K.; Curthois, J. J. *J. Chem. Soc. Faraday Trans.* **198**3, *1*, 805.
40. Filippidis, A.; Kantiranis, N. *Desalination* **2007**, *213*, 47–55.
41. Allen, S. J.; Ivanova, E.; Koumanova, B. *Chem. Eng. J.* **2009**, *152*, 389–395.
42. Barrer, R. M. *Can. J. Chem.* **1964**, *42*, 1480–1487.
43. Korkuna, O.; Leboda, R.; Skubiszewska-Zieba, J.; Vrublevska, T.; Gunko, V. M.; Ryczkowski, J. *Micropor. Mezopor. Mater.* **2006**, *87*, 243–254.
44. Ahmad, Z. B.; Dyer, A. In *Occurrence, Properties, and Utilization of Natural Zeolites*; Kallo, D.; Sherry, H. S., Eds. Akademiai Kiada: Budapest, Hungary, 1988, pp. 431–448.
45. Chelischev, N. F.; Bernshtein, B. G.; Volodin, V. F. *Natural Zeolites*; Metsniereba: Tbilisi, Georgia, 1979 (in Russian).
46. Pechar, F.; Rykl, D. *Chem. Pap.* **1987**, *41*, 351–362.
47. Breck, D. W. *Zeolite Molecular Sieves*; Wiley-Interscience: New York, NY, USA, 1974.
48. Elaiopoulos, K.; Perraki, T.; Grigoropoulou, E. *Micropor. Mesopor. Mater.* **2008**, *112*, 441–449.
49. Elaiopoulos, K.; Perraki, T.; Grigoropoulou, E. *Micropor. Mesopor. Mater.* **2010**, *134*, 29–43.
50. Ates, A.; Reitzmann, A.; Hardacre, C.; Yalcin, V. *Appl. Catal. A* **2011**, *407*, 67–75.
51. Vaculíková, L.; Plevová, E. *Acta Geodyn. Geomater.* **2005**, *2*, 167–175.
52. Elizalde-Gonzalez, M. P.; Mattusch, J.; Wennrich, R.; Morgenstern, P. *Micropor. Mesopor. Mater.* **2001,** *46*, 277–286.
53. Blanco-Varela, M. T.; Martinez-Ramirez, S.; Erena, I.; Gener, M.; Carmona, P. *Appl. Clay Sci.* **2006**, *33*, 149–159.
54. Sing, K. S. W.; Everett, D. H.; Haul, R. A. W.; Moscou, L.; Pierotti, R. A.; Rouquerol, J.; Siemieniewska, T. *Pure Appl. Chem.* **1985**, *57*, 603–619.
55. Munakata, K. *J. Nucl. Sci. Technol.* **2003**, *40*, 695–697.
56. Mockovčiaková, A.; Orolínová, Z.; Matik, M.; Hudec, P.; Kmecová, E. *Acta Montan. Slovaca Ročník* **200**6, *11*, 353–357.
57. Michelena, J. A.; Vansant, E .F.; De Bikvre, P. *Rec. Trav. Chim.* **1978**, *97*, 170–174.